Carbohydrate Polymers 381 (2026) 125198

Contents lists available at ScienceDirect

Carbohydrate Polymers

journal homepage: www.elsevier.com/locate/carbpol

Properties of agar aerogels: Effect of concentration and ageing time

Nika Atelšek Hozjan [a], Gabrijela Horvat [a], Lara Gibowsky [b], Pavel Gurikov [b,c,d], Željko Knez [a], Zoran Novak [a,*]

[a] Faculty of Chemistry and Chemical Engineering, University of Maribor, Smetanova ulica 17, 2000, Maribor, Slovenia
[b] Institute for Thermal Separation Processes, Hamburg University of Technology, Eißendorfer Straße 38, 21073, Hamburg, Germany
[c] Aerogel-it GmbH, Albert-Einstein-Str. 1, 49076, Osnabrück, Germany
[d] United Nations University Hub on Engineering to Face Climate Change at the Hamburg University of Technology, United Nations University Institute for Water, Environment and Health (UNU-INWEH), Eißendorfer Straße 38, 21073, Hamburg, Germany

ARTICLE INFO

Keywords:
Agar
Aerogel
Polysaccharide aerogel
Supercritical drying

ABSTRACT

Agar, a polysaccharide derived from red algae, is a renewable, edible, and biocompatible hydrocolloid with excellent gelling properties. Although widely used in the food industry and microbiology, its potential for advanced material design, particularly as an aerogel, has not yet been sufficiently explored. In this study, agar aerogels were produced via the sol-gel process and supercritical CO_2 drying. The effects of polysaccharide concentration (2%, 6%, and 10% w/v) and ageing time (24 h and 10 days) on the structural, textural and compressive mechanical properties were systematically investigated for the first time. All aerogels were highly porous, with specific surface areas reaching a maximum of 375 m^2/g at a moderate agar concentration (6% w/v). Prolonged ageing generally improved the textural and morphological properties but reduced the compression strength and swelling capacity. All samples showed excellent water uptake and remained stable in aqueous environments for four weeks. These results demonstrate that both concentration and ageing time significantly affect the final performance of the agar aerogels. Their properties can be easily adjusted by processing parameters, offering great potential for biomedical, food-related, or environmental applications.

1. Introduction

The rapid growth of the global population, depletion of natural resources, and harmful effects of synthetic materials on the environment have increased demand for biodegradable, versatile, and sustainable solutions (Advancement of Materials to Sustainable and Green World, n.d.; Correa et al., 2019). As a result, attention has focused on bio-based materials, which offer numerous benefits for society, the environment, and the economy (Bio-Based Products - European Commission, n.d.).

In this context, aerogels have emerged as a unique class of advanced porous materials. Recognised by IUPAC as one of the top ten emerging technologies in chemistry (Gomollón-Bel, 2022), aerogels are characterised by low density, high porosity, and low thermal conductivity. These properties make them attractive for applications ranging from thermal insulation (Guo et al., 2022; Zou & Budtova, 2021) and energy storage (Alwin & Sahaya Shajan, 2020; Mao et al., 2018) to biomedical applications (García-González et al., 2019; Karamikamkar et al., 2023) and environmental remediation. However, conventional silica aerogels have inherent limitations, including brittleness, which restricts their broader application. This has prompted increased investigation into bio-based aerogels (bioaerogels) (Hozjan et al., 2025), which combine the structural advantages of conventional silica aerogels with improved mechanical performance, biodegradability, non-toxicity, and enhanced functional versatility. Owing to these properties, bioaerogels present promising alternatives to current solutions in biomedical applications (García-González et al., 2019; Iglesias-Mejuto et al., 2024; Lázár et al., 2023; Veronovski et al., 2014), food packaging (Basak & Singhal, 2023; Selvasekaran & Chidambaram, 2022), and water purification (Paul & Ahankari, 2023). Despite these advantages, most bioaerogels remain at an early stage of development.

Among the various precursors used for bioaerogel production, polysaccharides are particularly attractive due to their natural abundance and gelling ability. Bioaerogels based on alginate (Dosta et al., 2019; Gurikov et al., 2015; Subrahmanyam et al., 2019), cellulose (Gavillon & Budtova, 2008; Paul & Ahankari, 2023), chitosan (Liao et al., 2024; Paul et al., 2024), and pectin (Groult & Budtova, 2018a; Horvat et al., 2015; Méndez et al., 2023) have been extensively studied and have demonstrated promising performance across multiple applications. In contrast, agar aerogels remain comparatively underexplored,

* Corresponding author.
E-mail address: zoran.novak@um.si (Z. Novak).

https://doi.org/10.1016/j.carbpol.2026.125198
Received 24 December 2025; Received in revised form 5 March 2026; Accepted 9 March 2026
Available online 10 March 2026

Abbreviations

BET	The Brunauer-Emmett-Teller theory
BJH	The Barrett-Joyner-Halenda model
DSC	Differential scanning calorimetry
SBF	Simulated body fluid
SEM	Scanning electron microscopy
TGA	Thermogravimetric analysis
TS	Total volumetric shrinkage
VS	Volumetric shrinkage

offering opportunities for further investigation.

Agar, extracted from red algae of the *Rhodophyceae* family, is a renewable and abundant biopolymer (Mostafavi & Zaeim, 2020). It consists of repeating 1,3-linked *β*-D-galactopyranose and 1,4-linked 3,6-anhydro-*α*-L-galactopyranose units, collectively known as agarobiose. Additionally, agar chains contain varying degrees of substitution, most commonly by methoxyl, sulphate ester, and pyruvate acetal groups. The type and extent of these substitutions depend on the algal species, strain, and environmental or physiological factors (Usov, 1998). The agarobiose (i.e. agarose) fraction is responsible for the characteristic gelling behaviour of agar (Bertasa et al., 2017). Agar dissolves in hot water and gels upon cooling below 35 °C, as the agarose chains transition from random coils to double helices, forming a three-dimensional network (Ayyad et al., 2010). Consequently, agar forms stable, robust gels over a wide concentration range (0.1–10% w/v) (Ayyad et al., 2010; Khoobbakht et al., 2024). Furthermore, agar is hydrophilic, biocompatible, and non-toxic, making it an ideal candidate for bioaerogel development, particularly for applications where environmental and human safety are paramount.

Polysaccharide-based aerogels are typically produced using the sol-gel process followed by supercritical drying. This method involves gelation, solvent exchange, and ageing, all of which are essential steps for preserving the integrity of the porous gel network during supercritical drying (Smirnova and Gurikov, 2018). The final properties of these materials depend not only on the process itself but also on parameters such as precursor concentration, solvent exchange, and ageing conditions (Payanda Konuk et al., 2023). Biopolymer concentration determines network density and porosity, thereby influencing textural and mechanical properties. Higher biopolymer concentrations generally result in increased density and improved mechanical properties (Gavillon & Budtova, 2008), while lower concentrations promote greater porosity and potentially higher specific surface areas (Payanda Konuk et al., 2023). Ageing promotes cross-linking of biopolymer chains and densification of the gel network, but may also cause adverse effects, such as reduced pore size or mechanical strength (Ratke & Gurikov, 2021). Despite their significance, these parameters are often studied independently, and their combined effect on polysaccharide-based aerogels remains insufficiently understood.

Only a limited number of studies have addressed agar aerogels. Robitzer et al. reported the preparation of agar aerogel beads (2% w/v) and demonstrated, using gas physisorption, that these materials possess predominantly macroporous structures with high specific surface area (>300 m^2/g) (Robitzer, Renzo, & Quignard, 2011; Robitzer, Tourrette, et al., 2011). Athamneh et al. later evaluated agar aerogel discs in vivo, showing promising performance in wound healing (Athamneh et al., 2023). More recently, Keil et al. reported the production of agar aerogel powder and demonstrated its potential for life science applications through swelling and biocompatibility studies (Keil et al., 2024). However, these studies focus on specific material forms and applications, and do not provide a systematic understanding of how processing parameters influence material properties. In particular, the combined effect of agar concentration and ageing time on the structural, textural and compressive mechanical properties of agar aerogels has not yet been systematically investigated. This lack of understanding limits the ability to establish a clear structure-property relationship and hinders the rational design of these materials.

In this study, we aimed to address this gap by investigating the influence of agar concentration (2%, 6%, and 10% w/v) and ageing time (24 h versus 10 days) on the properties of agar aerogels. A single-step solvent exchange to absolute ethanol was used to assess its effectiveness and limitations in producing structurally stable materials. The selected ageing conditions were intended to capture the extremes of network evolution during solvent exchange. Textural, morphological, structural, and compressive mechanical properties were systematically evaluated, along with swelling and stability tests in aqueous media (distilled water and simulated body fluid (SBF)). It is hypothesised that agar concentration and ageing time govern the formation and reorganisation of the gel network, enabling controlled tuning of agar aerogel properties for targeted applications.

2. Materials and methods

2.1. Materials

Agar (for bacteriology, purity ≥99%, CAS: 9002-18-0, $M_W = 71$ kDa, gel strength >750 cm/g^2, total ash content 2.8%, moisture content 7.2%, gelling temperature 34.5 °C, melting temperature 88 °C, as determined by the supplier at a concentration of 1.5%) was purchased from Biolife Italiana (Milan, Italy). The agarose/agaropectin ratio of agar is 71.2/28.8, as determined using the existing method (Jeon et al., 2005). Additional characterisation of agar (molecular weight determination, FTIR analysis, and high-temperature NMR analysis) is described in the Supplementary material (Section S1).

Anhydrous absolute ethanol, C_2H_5OH (purity ≥99.5%), was obtained from Carlo Erba (Milano, Italy). Sodium chloride, NaCl (purity ≥99.8%, CAS number: 7647-14-5), anhydrous magnesium chloride, $MgCl_2$ (purity ≥98.0%, CAS: 7786-30-3) and calcium chloride dihydrate, $CaCl_2{\cdot}2H_2O$ (for analysis, CAS: 10035-4-8), were purchased from Sigma-Aldrich (Darmstadt, Germany). Carbon dioxide, CO_2 (purity by volume 99.5%), was obtained from Messer (Ruše, Slovenia). Sodium hydrogen carbonate, $NaHCO_3$ (for analysis, CAS: 144-55-8) and sodium sulfate, Na_2SO_4 (purity ≥99.0%, CAS: 7757-82-6), were acquired from Merck KGaA (Darmstadt, Germany). Potassium chloride, KCl (purity ≥99.5%, CAS: 7447-40-7) and hydrochloric acid, HCl (≥37.0%) were purchased from Honeywell (Seelze, Germany). Tris(hydroxymethyl) aminomethane, $NH_2C(CH_2OH)_3$ (primary standard and buffer, purity ≥99.9%, CAS: 77-86-1) was obtained from Sigma-Aldrich (St. Louis, USA). Anhydrous potassium hydrogen phosphate, K_2HPO_4 (purity ≥98.0%, CAS: 7758-11-4), was acquired from Kemika (Zagreb, Croatia). All reagents were used as received.

Ultra-pure water (18.2 MΩ cm at 25 °C), produced by the Milli-Q® system (EMD Millipore Corporation, USA), was used to prepare SBF. Distilled water was used in all other experiments.

SBF was prepared according to the protocol of Kokubo (Kokubo et al., 1990).

2.2. Preparation of agar aerogels

2.2.1. Synthesis of agar alcogels

Agar alcogels were prepared by the sol-gel process, as shown in Scheme 1. Briefly, agar powder (0.8, 2.4, and 4.0 g) was dispersed in distilled water (40 mL) in a beaker to obtain solutions of 2%, 6%, and 10% w/v. The dispersions were mixed for 10 min at room temperature (25 °C) to ensure the polysaccharide was hydrated. The beaker was then covered and placed in a preheated oil bath (110 °C), brought to the boil, and stirred (400 rpm) until the agar was completely dissolved and a clear solution was obtained. The beaker containing the hot agar solution was then placed in a heated ultrasonic bath (70 °C) and sonicated (15

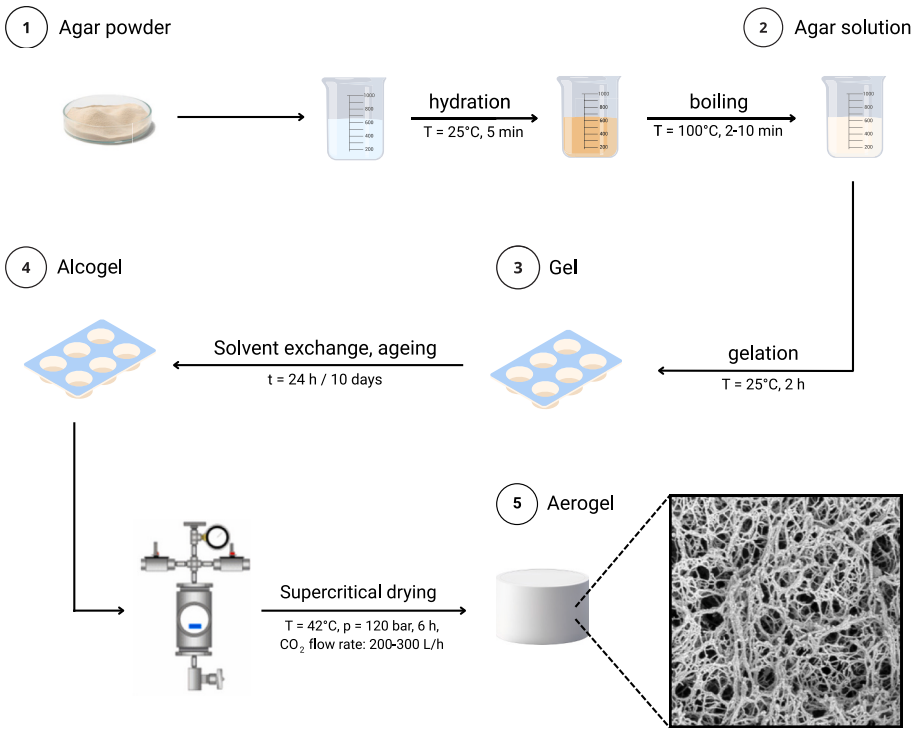

Scheme 1. Schematic illustration of the agar aerogel synthesis process.

min) to remove trapped air bubbles. The hot agar solution was poured into cylindrical moulds (20 mm diameter × 15 mm height) and left to cool to room temperature (25 °C) for at least 1 h to form a gel. Once gel formation was complete, the hydrogels were carefully removed from the moulds and immersed in absolute ethanol to initiate the exchange of water with alcohol. Ageing in ethanol was carried out for 24 h or 10 days, with the ethanol being replaced several times. This step transformed the hydrogels into alcogels.

2.2.2. Supercritical drying with CO_2

Agar alcogels were supercritically dried with CO_2 in a modified supercritical extraction unit (UHDE GmbH, Dortmund, Germany), following a previously developed method (Novak & Knez, 1997). A 500 mL autoclave was filled with absolute ethanol, and the samples were immersed. The system was then heated to 42 °C and pressurised to 120 bar at a controlled rate (2 bar/min). The supercritical drying process was carried out for 6 h at a constant CO_2 flow rate of 20–30 L/h (determined at 0.984 bar and 23 °C). After the drying process was completed, the system was depressurised to atmospheric pressure at 5 bar/min while maintaining a temperature of 42 °C. The resulting aerogels were removed from the autoclave and stored in plastic containers sealed with Parafilm. They were placed in a desiccator until further analysis.

2.3. Characterisation of agar aerogels

2.3.1. Volumetric shrinkage

The volumetric shrinkage (VS) of the agar aerogels was determined after ageing in ethanol and calculated according to Eq. (1), where V_{AL} is the volume of the agar alcogel before drying and V_A is the volume of the agar aerogel. The total volumetric shrinkage (TS) was determined after supercritical drying and calculated using Eq. (2), where V_H is the volume of the agar hydrogel, and V_A is the volume of the agar aerogel. The volumes were measured using a digital calliper (ABS, HOLEX, Germany) with a measurement error of ±10%.

$$VS(\%) = \frac{V_{AL} - V_A}{V_{AL}} \times 100 \quad (1)$$

$$TS(\%) = \frac{V_A - V_H}{V_H} \times 100 \quad (2)$$

All measurements were performed in triplicate, and the mean ± standard deviation is reported.

2.3.2. Density and porosity

The bulk density (ρ_b) of the aerogels was measured using a bulk density analyser (GeoPyc 1365, Micromeritics Instrument Corporation, USA).

The skeletal density (ρ_s) was determined with helium gas pycnometer (Accupyc II 1340 Pycnometer, Micromeritics Instrument Corporation, USA). Ten data points were collected, and ten equilibrium cycles were recorded. The porosity of the aerogels (Π) was then calculated from ρ_b and ρ_s using Eq. (3).

$$\Pi(\%) = \left(1 - \frac{\rho_b}{\rho_s}\right) \times 100 \quad (3)$$

The total pore volume (V_{TOT}) and average pore diameter (Φ) were calculated using Eqs. (4) and (5), respectively, where S_{BET} represents the specific surface area obtained from N_2 physisorption analysis.

$$V_{TOT} = \left(\frac{1}{\rho_b} - \frac{1}{\rho_s}\right) \quad (4)$$

$$\Phi = 4 \times \frac{V_{TOT}}{S_{BET}} \quad (5)$$

All measurements were performed in triplicate, and the mean ± standard deviation is reported.

2.3.3. N_2 physisorption analysis

The textural properties of the agar aerogels were analysed using N_2 physisorption. The specific surface area (m^2/g) was calculated using the Brunauer-Emmett-Teller (BET) theory from the linear region of the adsorption isotherm in the 0.06–0.35 relative pressure (p/p^0) range, while the average mesopore volume (V_{BJH}), average mesopore size (d_{BJH}), and pore size distribution were derived from the desorption

branch of the isotherm using the Barrett-Joyner-Halenda (BJH) model. Adsorption isotherms were also plotted. Before analysis, the samples (approx. 0.05 g) were degassed under vacuum at 60 °C for 12 h and then analysed at −196 °C. All measurements were performed using a porosity analyser (ASAP 2020 MP, Micromeritics Instrument, Norcross, GA, USA).

All measurements were performed in triplicate, and the mean ± standard deviation is reported.

2.3.4. Scanning electron microscopy analysis (SEM)

The morphological characterisation of the agar aerogels was carried out using SEM. Before imaging, the samples were cut into small pieces and sputter-coated with a 5 nm gold layer. They were then placed on the sample holder and secured with copper tape. The samples were scanned at an accelerating voltage of 2 kV with magnifications of 50,000× and 80,000×. The analysis was conducted using the Helios™ G4 PFIB CXe DualBeam™ FIB/SEM microscope (Thermo Fisher, Massachusetts, USA) with a TLD detector. The images were analysed with ImageJ (FIJI, software version 1.54p; U.S. National Institutes of Health, Bethesda, MD, USA).

2.3.5. Thermal analyses

The thermal properties of the agar aerogels were evaluated by thermogravimetry (TGA) and differential scanning calorimetry (DSC). Both analyses were conducted under an air atmosphere at a heating rate of 10 °C/min over the range 30 to 600 °C. Measurements were performed using a TGA/DSC device (TGA/DSC1 Star System, Mettler Toledo, Switzerland). TGA and DSC curves were recorded. Approximately 10 mg of each sample was used.

All measurements were performed in duplicate, and the mean ± standard deviation is reported.

2.3.6. Wettability measurement

The wettability of the agar aerogels was assessed using the sessile drop method on a contact angle analyser (OCA25, Data-Physics, Germany). A drop of ultrapure water (1 μL) was deposited on the surface of the aerogel, and the time taken for complete absorption into the material was recorded. The contact angle was determined using dpiMAX software (version 2.0.118, DataPhysics, Germany). Measurements were carried out under standard room conditions (25 ± 1 °C; 40% relative humidity).

2.4. Behaviour in aqueous media

The behaviour of the agar aerogels in aqueous media was evaluated by assessing their swelling capacity, following a previously established method (Pantić et al., 2024). The analysis was conducted in distilled water and SBF.

To determine the swelling capacity, the agar aerogels were cut into smaller pieces, weighed (0.01 g) and immersed in vials containing either distilled water or SBF (20 mL) at room temperature (25 ± 0.5 °C). At predetermined time intervals (15, 30, and 45 min; 1, 2, 4, 8, 24, and 48 h; and 1, 2, 3, and 4 weeks), samples were removed, carefully blotted with laboratory paper to remove excess liquid and weighed using an analytical balance (XPE205/M, Mettler Toledo, Switzerland). The swelling ratio was calculated using Eq. (6), where w_{WET} is the mass of wet aerogels at time t, and w_{DRY} is the initial dry mass of the aerogels. After weighing, the samples were returned to the vials.

$$\text{Swelling ratio}(\%) = \frac{w_{WET} - w_{DRY}}{w_{DRY}} \times 100 \quad (6)$$

All measurements were performed in triplicate, and the mean ± standard deviation is reported.

2.5. Uniaxial compression test

To evaluate the compressive mechanical strength of the agar aerogel samples, uniaxial compression tests were performed using a texture analyser (TA.XTplusC, Stable Micro Systems, Godalming, UK). Before measurements, the alignment of the sample and plate was adjusted to ensure even load distribution. The samples, with varying thicknesses (approximately 15 × 12 mm), were compressed using a flat compression plate with a 30 mm diameter. Forces of 100 N (2% w/v agar aerogels), 200 N (6% w/v agar aerogels), and 450 N (10% w/v agar aerogels) were applied, with a constant probe speed of 1 mm/s. Measurements were conducted under normal indoor room conditions (23 ± 1 °C; 40% relative humidity).

During compression, the force (F) and displacement (d) were continuously recorded. Strain was manually calculated as the ratio of displacement to the initial height, while stress was determined using the initial cross-sectional area measured before testing. The tests continued until the specified maximum load capacity was reached. The compressive modulus was calculated over a 3–8% strain range for all samples to determine the slope of the first linear portion of the compressive stress-strain curve. To avoid measurement artefacts caused by the uneven surface of the monolithic samples, the initial strain range of 0–3% compression was excluded from the modulus calculation.

Four replicates were performed for each sample, and the mean ± standard deviation is reported.

To evaluate the energy absorption capacity of the prepared aerogels under compression, the energy absorption capacity was determined by integrating the compression stress–strain curves using the trapezoidal rule. As no breakage point was observed in the samples, the absorbed energy was calculated at predefined strain levels of 10% and 30% (when applicable). The resulting energy density was multiplied by the sample volume to obtain the total absorbed energy (kJ). Reported values represent the mean ± standard deviation of four replicates.

2.6. Statistical analysis

Three separate batches of agar aerogels were produced, and all experiments and analyses were performed in triplicate unless otherwise stated. All experimental data are reported as mean ± standard deviations.

3. Results and discussion

A comprehensive characterisation was performed to evaluate the effects of agar concentration and ageing time on the structure-property relationships of agar aerogels. Physical properties, including appearance, shrinkage, density, and porosity, were examined to assess structural changes in the gel network that occurred during processing. Textural properties were probed using N_2 physisorption analysis, while SEM provided visualization of the microstructure and morphological differences between the samples. Thermal stability and decomposition behaviour were examined using TGA/DSC analyses. Surface properties and behaviour in aqueous media were evaluated to determine wettability and swelling ratio. Finally, mechanical compression testing was performed to assess the compression strength and deformation characteristics of the agar aerogels.

3.1. Characterisation of agar aerogels

3.1.1. Visual observations, shrinkage, density and porosity

Agar solutions were prepared by dissolving the polysaccharide in boiling water (100 °C). As the agar concentration increased, the solutions became very viscous, making gel casting more challenging. Air bubbles formed in the solution during boiling. To minimise this issue, the hot agar solutions were kept in a water bath at 70 °C and treated with ultrasound for 15 min. While this method successfully removed air bubbles from the 2% and 6% w/v solutions, some remained in the 10% w/v solution. This may have affected the homogeneity and properties of the final aerogels. The resulting aerogels were labelled **XAY**, where **X**

refers to the agar concentration in % w/v (2, 6 and 10), **A** refers to the agar aerogel, and **Y** refers to the ageing time in absolute ethanol, where 1 represents 1 day (24 h), and 10 represents 10 days. For example, 2A1 refers to a 2% w/v agar aerogel that was aged in ethanol for 1 day, while 10A10 refers to a 10% w/v agar aerogel that was aged for 10 days.

Images of agar hydrogels and their corresponding aerogels are shown in Fig. 1. Supercritical drying of agar alcogels resulted in white monoliths that were neither brittle nor fragile. Aerogels containing 2% w/v agar appeared soft and spongy and were easily compressible; in contrast, aerogels containing 6% and 10% w/v were firmer and more rigid. These observations align with the mechanical behaviour of the aerogels discussed in Section 3.3, where a higher agar concentration corresponded to higher compressive strength and modulus. It is noteworthy that agar aerogels at 2% w/v concentration exhibited non-uniform shrinkage, with a visible deformation in the centre of the sample. This was due to compaction of the biopolymer chains, as previously reported for agar gels (Hajnal et al., 2023). The deformation decreased with increasing concentration; agar aerogels at 10% w/v retained their original shape.

To demonstrate the importance of the drying method for preserving the gel structure, images of agar xerogels (i.e. gels dried under ambient conditions) are provided in the Supplementary material (Fig. S1). Xerogels exhibited severe shrinkage and complete deformation, confirming that supercritical drying is essential to maintaining the structural integrity and shape of agar gels during aerogel production.

Volumetric shrinkage was determined at all stages of the processing. A comprehensive summary of the results is provided in Table 1 and presented in Fig. 2. Minor volumetric shrinkage was observed after the solvent exchange, with values decreasing from 2.46% to 1.82% after 1 day and from 3.04% to 2.82% after 10 days of ageing as concentration increased. The most significant volumetric shrinkage occurred during the supercritical drying. It was strongly concentration-dependent, ranging from 76% (sample 2A1) to 25% (sample 10A10). However, prolonged ageing time reduced shrinkage by an average of 10–20%. These results are comparable to those reported for other aerogels with low polymer content, whose structures tend to collapse due to a fragile network that cannot fully withstand the internal stresses induced by the drying process (Payanda Konuk et al., 2023; Subrahmanyam et al., 2015). In contrast, denser networks were formed at higher agar concentrations, making those aerogels more resistant to shrinkage due to the greater number of hydrogen bonds between the polysaccharide chains. Similar trends have been reported for other biobased aerogels, namely chitosan (Chartier et al., 2022), pectin (Méndez et al., 2023) and cellulose (Buchtová & Budtova, 2016; Karadagli et al., 2015). Notably, samples that shrank substantially (2A1 and 2A10) retained exceptional porosity (>96%), a phenomenon previously observed in cellulose

Table 1
Total volumetric shrinkage (TS), bulk density (ρ_b), and porosity (Π) of agar aerogels.

Sample[a]	TS (%)[b]	ρ_b (g/cm^3)	Π (%)[c]
2A1	76.0 ± 0.8	0.06 ± 0.01	96
2A10	68.4 ± 0.7	0.04 ± 0.01	97
6A1	49.7 ± 1.6	0.12 ± 0.01	91
6A10	43.6 ± 2.1	0.10 ± 0.01	92
10A1	35.5 ± 0.8	0.19 ± 0.01	84
10A10	25.6 ± 0.6	0.18 ± 0.01	85

[a] XAY, where X = agar concentration (% w/v), A = agar aerogel, and Y = ageing time (1 = 24 h; 10 = 10 days).
[b] Calculated based on dimensional changes of the samples (n = 3).
[c] Calculated using equation: $\Pi = (1\text{-}\rho_b/\rho_s) \times 100\%$.

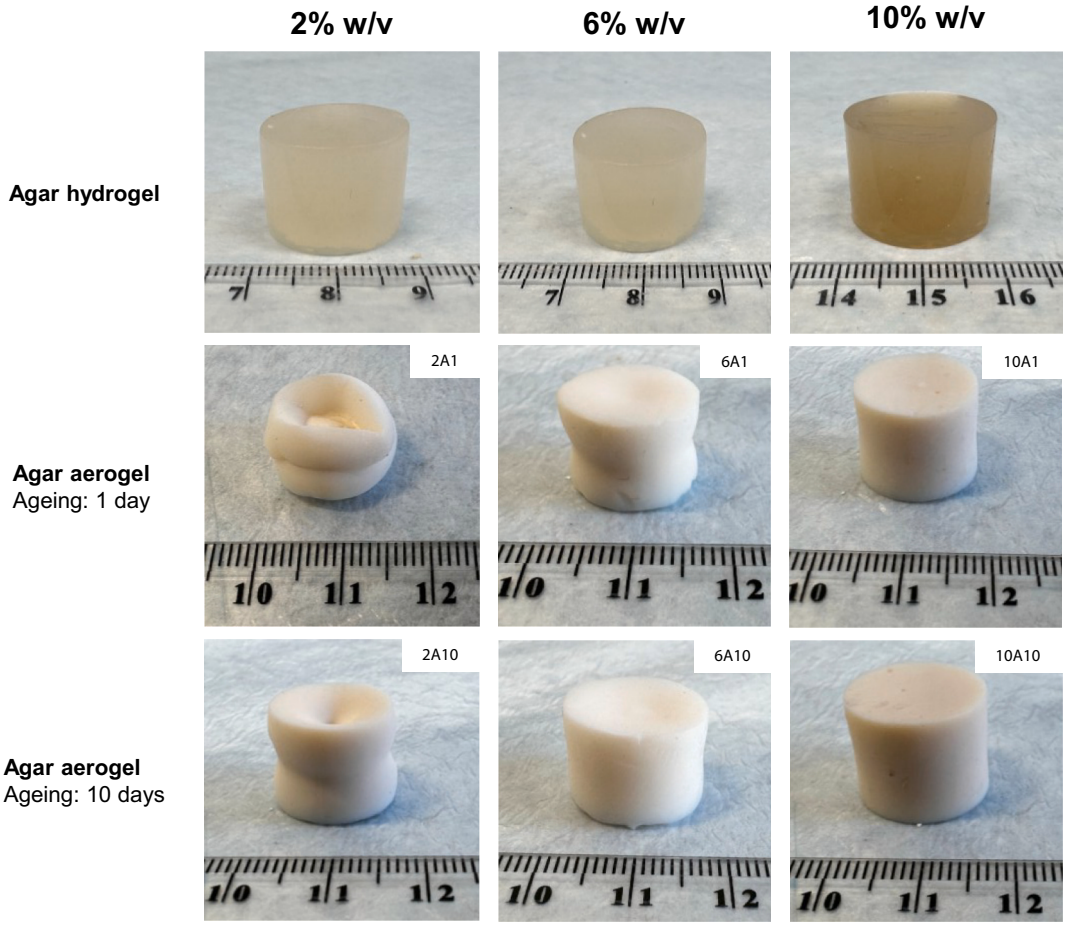

Fig. 1. Visual appearance of agar hydrogels and corresponding agar aerogels.

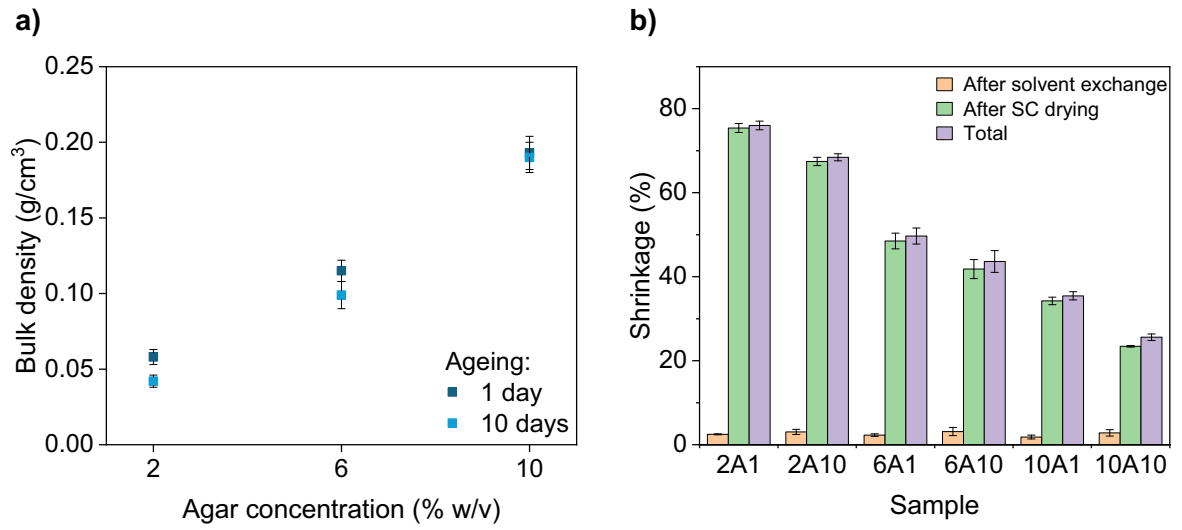

Fig. 2. a) Bulk density of agar aerogels as a function of agar concentration and ageing time, and b) VS of agar aerogels at different processing stages: after solvent exchange (orange), after supercritical drying (green), and TS (purple).

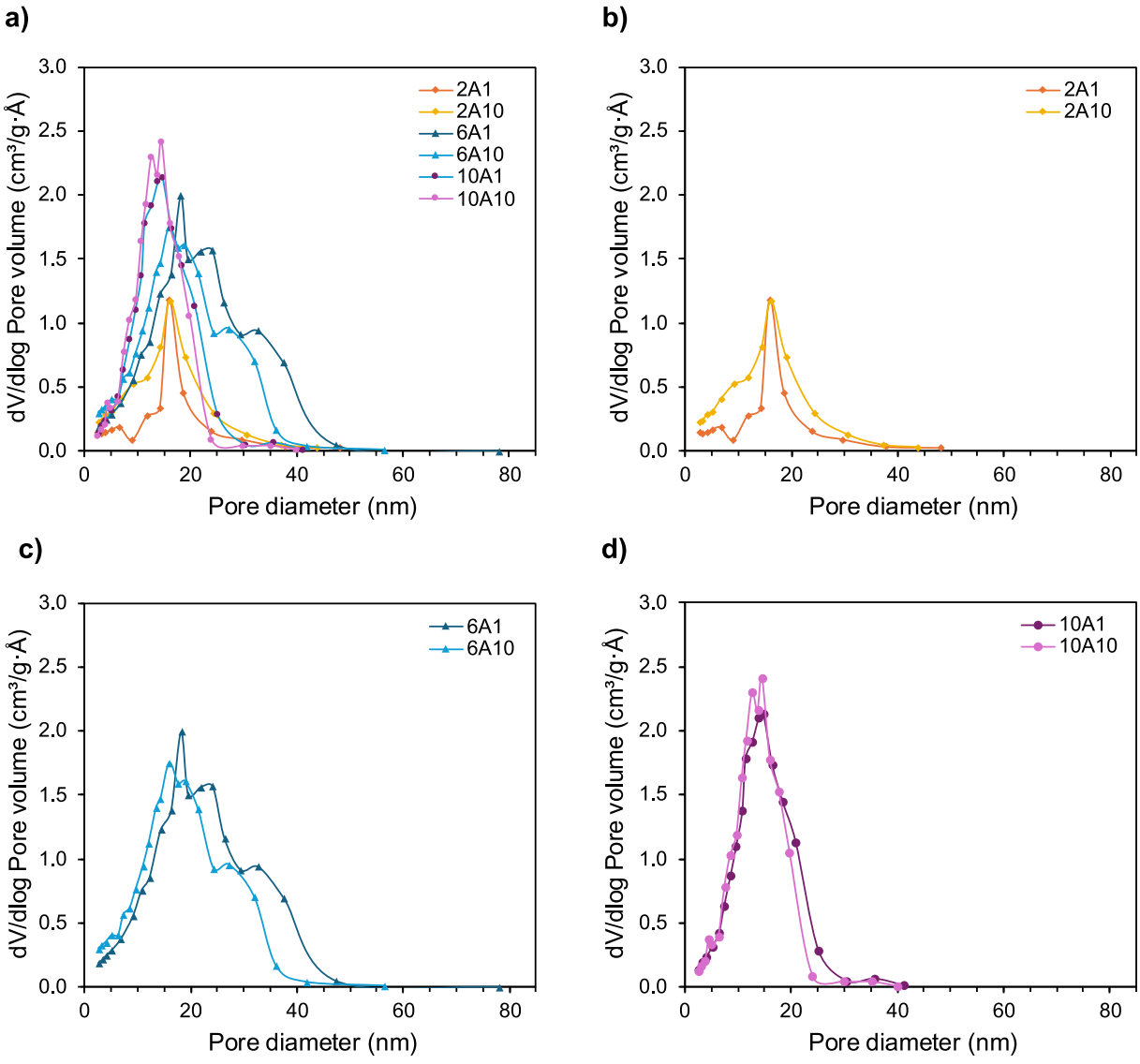

Fig. 3. BJH pore size distribution for a) all agar aerogels, b) 2% w/v agar aerogels, c) 6% w/v agar aerogels and d) 10% w/v agar aerogels.

aerogels (Buchtová & Budtova, 2016).

Visual observation of the samples revealed that the gel's core contracts upon direct exposure to absolute ethanol, particularly at a low concentration of 2% w/v, as previously observed in the literature (Hajnal et al., 2023). It is hypothesised that this central compaction is due to mechanical compression from the edges towards the centre, as well as the interactions between the solvent and polymer. The denser, mechanically stronger edges that formed during gelation can therefore resist shrinkage more effectively than the gel's centre. However, combining a one-step solvent exchange with an extended ageing time reduced this effect, ultimately producing dimensionally stable aerogels.

The bulk density and porosity of the agar aerogels were strongly affected by both the agar concentration and the ageing time (Table 1, Fig. 2). Increasing the agar concentration from 2% to 10% w/v resulted in a substantial increase in bulk density (from 0.06 to 0.18 g/cm^3) and a corresponding decrease in porosity (from 96% to 84%), which can be attributed to denser network formation due to a higher solids content. Similar trends have been reported for other polysaccharide-based aerogels, including pectin (Groult & Budtova, 2018b), chitosan (Chartier et al., 2022) and cellulose (Buchtová & Budtova, 2016). Extending the ageing time from 1 to 10 days resulted in a decrease in bulk density and a slight increase in porosity across all tested concentrations. For example, the bulk density in sample 2A decreased from 0.06 to 0.04 g/cm^3, while the porosity increased from 96% to 97%. Similar trends were observed in samples 6A (0.12 → 0.10 g/cm^3; 91% → 92%) and 10A (0.19 → 0.18 g/cm^3; 84% → 85%). This behaviour suggests that prolonged ageing time facilitates the gradual relaxation of the network and the reorganisation of the polymer chains, thereby better preserving the open pore structure during supercritical drying, as observed in other bioaerogels (Payanda Konuk et al., 2023). The observed reduction in bulk density and total shrinkage, along with the increased porosity, suggests that the network's structural integrity is maintained. At the same time, the internal microstructure becomes more porous.

3.1.2. N_2 physisorption analysis

The textural properties of the agar aerogels were analysed using N_2 physisorption. The specific surface areas were calculated using the BET method, while the average mesopore diameters (d_{BJH}) and volumes (V_{BJH}) were determined using the BJH model. Additionally, the pore size distributions (Fig. 3) and adsorption isotherms (Fig. 4) were plotted. The results are summarised in Table 2.

With increasing agar concentration from 2% to 6% w/v, the average mesopore diameter also increased, reaching a maximum (11.98 nm) in the sample 6A1. This concentration overcomes the limitations observed in agar aerogels of 2% and 10% w/v, where pore development is hindered by low network strength or excessive compaction, respectively. Similar trends have been reported for other polysaccharide-based aerogels, such as pectin (Groult & Budtova, 2018b) and cellulose (Buchtová & Budtova, 2016). Additionally, prolonged ageing time generally led to a decrease in the average mesopore diameter, probably due to further

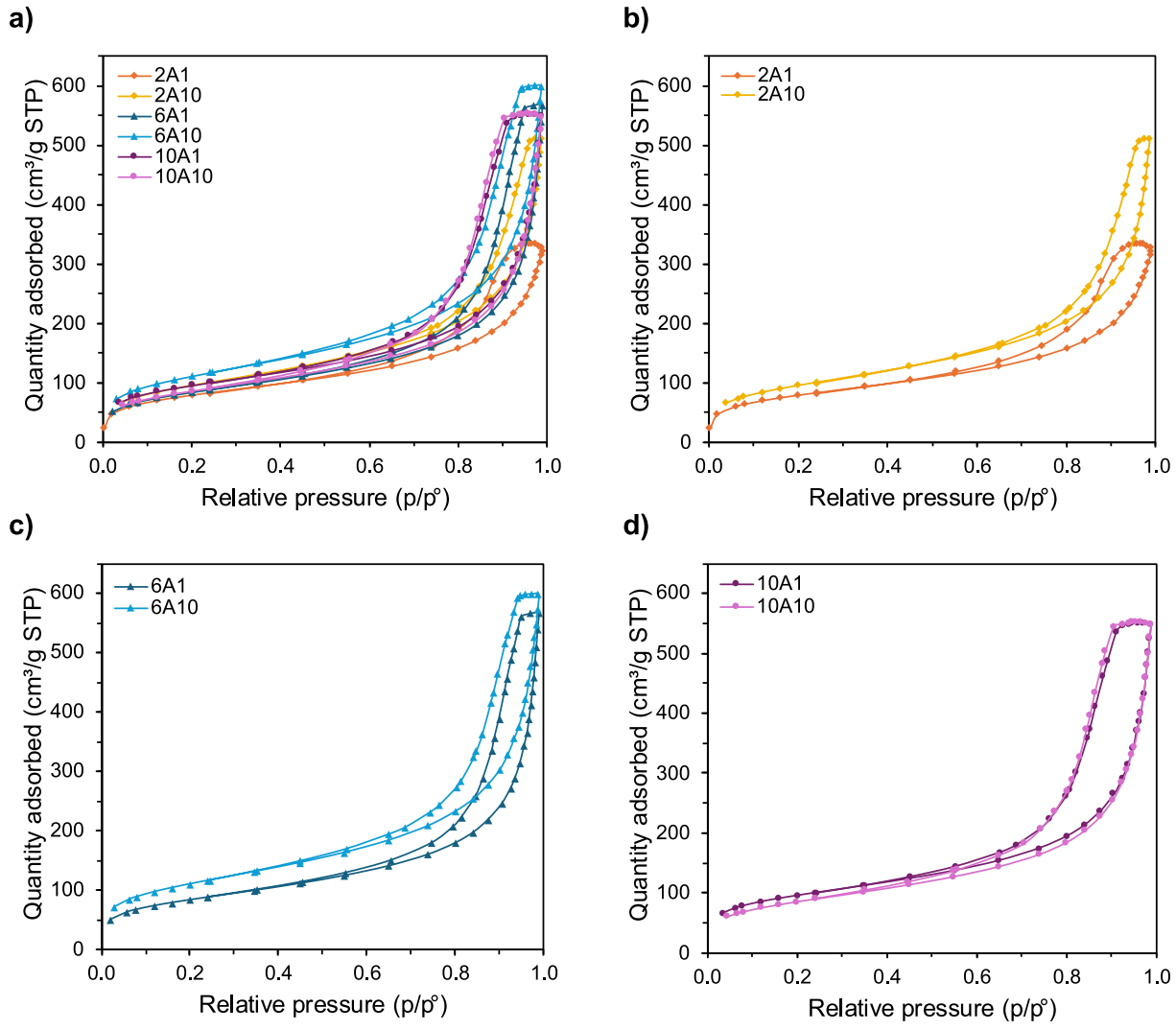

Fig. 4. Adsorption-desorption isotherms for a) all agar aerogels, b) 2% w/v agar aerogels, c) 6% w/v agar aerogels and d) 10% w/v agar aerogels.

Table 2
Average mesopore diameter (d_{BJH}), average pore diameter (Φ), average mesopore volume (V_{BJH}), total pore volume (V_{TOT}) and specific surface area (S_{BET}) of agar aerogels.

Sample[a]	d_{BJH} (nm)[b]	V_{BJH} (cm^3/g)[b]	S_{BET} (m^2/g)[c]	V_{TOT} (cm^3/g)[d]	Φ (nm)[e]
2A1	8.47 ± 0.11	0.29 ± 0.03	182 ± 5	16.55	364
2A10	9.12 ± 0.15	0.34 ± 0.01	265 ± 7	23.14	350
6A1	11.65 ± 0.33	0.89 ± 0.01	284 ± 6	7.92	112
6A10	10.06 ± 0.18	0.93 ± 0.02	375 ± 8	9.26	99
10A1	10.23 ± 0.21	0.87 ± 0.05	314 ± 8	4.35	55
10A10	9.83 ± 0.54	0.74 ± 0.10	291 ± 6	4.72	65

[a] XAY, where X = agar concentration (% w/v), A = agar aerogel, and Y = ageing time (1 = 24 h; 10 = 10 days).
[b] Extrapolated from the desorption branch of the isotherms using the BJH method (Horvat et al., 2022) ($n = 3$).
[c] Calculated based on the BET theory ($n = 3$).
[d] Calculated using equation: $V_{TOT} = (1/\rho_b) - (1/\rho_s)$ from the mean value.
[e] Calculated using equation: $\Phi = (4 \times V_{TOT})/S_{BET}$ from the mean value.

densification of the polymer network.

The specific surface areas were high across all samples, with a slight upward trend as agar concentration and ageing time increased. Sample 6A10 had the highest BET value (375 m^2/g), which supports the hypothesis that a moderate agar concentration combined with a prolonged ageing time improves the structural properties of the aerogels. However, a prolonged ageing time led to a slight decrease in the specific surface area of the sample 10A10 (from 314 m^2/g to 291 m^2/g), confirming that a high polymer content forms a stronger network, which prevents further coarsening of the pores. These results are consistent with previous research (Groult & Budtova, 2018b), which suggests that increasing polymer concentration generally results in smaller pores. In contrast, the thickness of the pore walls remains mostly unchanged—in other words, adding more material results in larger pores being divided into smaller ones.

The samples exhibited a hierarchical porosity, consisting of both smaller and larger pores in the mesoporous region (Fig. 3a), as well as macropores, as revealed by SEM examination (Fig. 5). This structure was most evident in sample 6A (Fig. 3c), which exhibited a bimodal pore size distribution with peaks at 18 and 35 nm, typical of well-developed mesoporous materials. In contrast, the samples containing 2% w/v agar showed a narrow distribution in the 5–20 nm range (Fig. 3b). In the samples containing high polysaccharide concentration (10% w/v, the hierarchical porosity was almost completely absent (Fig. 3d). Moreover, micropores (<2 nm) accounted for only a small proportion (<3%) of the total surface area in all samples. These microporous regions likely originated from localised ordering or denser zones within the polymer network, resulting from hydrogen bonding or chain entanglement formed during gelation and ageing.

The BJH pore size distribution shows the presence of mesopores (2–50 nm) in all agar aerogels, with mesopore volumes ranging from 0.29 cm^3/g (sample 2A1) to 0.93 cm^3/g (sample 6A10). However, the total pore volumes, determined from bulk and skeletal densities, are substantially larger, ranging from 4.35 cm^3/g (sample 10A1) to 23.14 cm^3/g (sample 2A10), indicating that all agar aerogels are predominantly macroporous. The mesoporous fractions of the samples (determined with N_2 physisorption analysis and the BJH model), therefore, represent only 1.5–20% of the total pore volume, depending on the sample. This is further supported by the average pore diameters (Table 2), which are well within the macroporous range (>50 nm). Results on the porosity and textural properties obtained for agar aerogels are consistent with those of other polysaccharide aerogels (Robitzer et al., 2008; Robitzer, Tourrette, et al., 2011).

The N_2 adsorption-desorption isotherms (Fig. 4) displayed typical IV curves, indicating the presence of mesoporous domains (2–50 nm) in all agar aerogels (Sing, 1982). According to the IUPAC classification, the hysteresis loops were either of type H1 (samples 2A10, 6A1, 6A10, 10A1 and 10A10) or H2(b) (sample 2A1), reflecting differences in pore structure (Thommes et al., 2015). The H2(b) loop observed in sample 2A1 (Fig. 4b) likely resulted from a weak polymer network that partially collapsed due to internal stress during supercritical drying, forming irregularly shaped pores with narrow necks and wider bodies, commonly referred to as "ink-bottle shapes" (Thommes et al., 2015). This morphology hindered N_2 desorption, delayed gas release, and widened hysteresis (Cychosz & Thommes, 2018). With prolonged ageing time, the adsorption-desorption isotherm shifted upwards, indicating increased N_2 uptake due to improved pore accessibility. Contrarily, the H1 loops observed in Fig. 4c and d are characteristic of more uniform, cylindrical mesopores (Horvat et al., 2022; Thommes et al., 2015). These samples displayed nearly parallel adsorption and desorption branches, indicating efficient gas exchange and well-preserved pore structure. Prolonged ageing time enhanced this effect in sample 6A10, resulting in smaller pore sizes and a higher BET (Table 2). However, in 10% w/v aerogels (Fig. 4d), the adsorption-desorption capacity remained unchanged, indicating that the structure and total pore volume were preserved. These results implied that ageing at this concentration has only a limited effect on the overall shape and size of the pores.

3.1.3. SEM

SEM analysis was performed on all samples except 2A1, which was excluded due to severe shrinkage and shape deformation after supercritical drying (Fig. 1). The SEM images (Fig. 5) revealed that agar aerogels possess a fibrillar morphology, with no visible heterogeneity, large voids, or aggregated areas. SEM analysis also confirmed a uniform network structure and the presence of interconnected meso- and macropores ranging from approximately 10 to 300 nm, consistent with the N_2 physisorption results.

The morphology was strongly influenced by the polymer concentration. Using a low agar concentration (sample 2A10) resulted in a highly porous network with large, irregularly shaped pores. Increasing the agar concentration resulted in denser, more homogeneous fibrillar structures with reduced pore diameters and an increased specific surface area, as determined with BET and BJH models (Table 2).

The ageing time also influenced the morphology. Comparisons between samples 6A1 and 6A10, as well as between 10A1 and 10A10, showed that extended ageing led to more compact structures with smaller pores, likely due to the complete replacement of solvent, which reduced water-mediated solvation and enhanced polymer–polymer interactions. SEM images further revealed the predominantly macroporous nature of the agar aerogels. Overall, SEM imaging provided clear evidence of the structural tunability of agar aerogels, demonstrating that porosity and morphology can be modulated by adjusting both agar concentration and ageing time.

3.1.4. Thermal analysis

The thermal stability of the samples was examined through TGA and DSC analyses. The results are summarised in Table 3 and Fig. 6.

Aerogels are highly porous, which means they often retain residual solvents. Their hydrophilic nature also makes them prone to absorbing moisture from the surrounding environment. Consequently, thermal analyses typically show an initial mass loss step between 80 and 100 °C, corresponding to the evaporation of volatile components and physically adsorbed water. Within this temperature range, materials generally lose between 10% and 20% of their original mass (Horvat et al., 2017). A similar trend was observed in this study, with a mass loss of 10–12% occurring between 87 °C and 144 °C (Fig. 6a). This aligns with recent data reported for agar aerogel powder (Keil et al., 2024). However, this step involves removing adsorbed moisture from the air and is not correlated with the material's mass loss due to degradation. The severe weight loss occurred at ≈260 °C, at which all samples lost approximately 60% of their total mass, regardless of agar concentration or ageing time. This significant decomposition step is attributed to the thermal

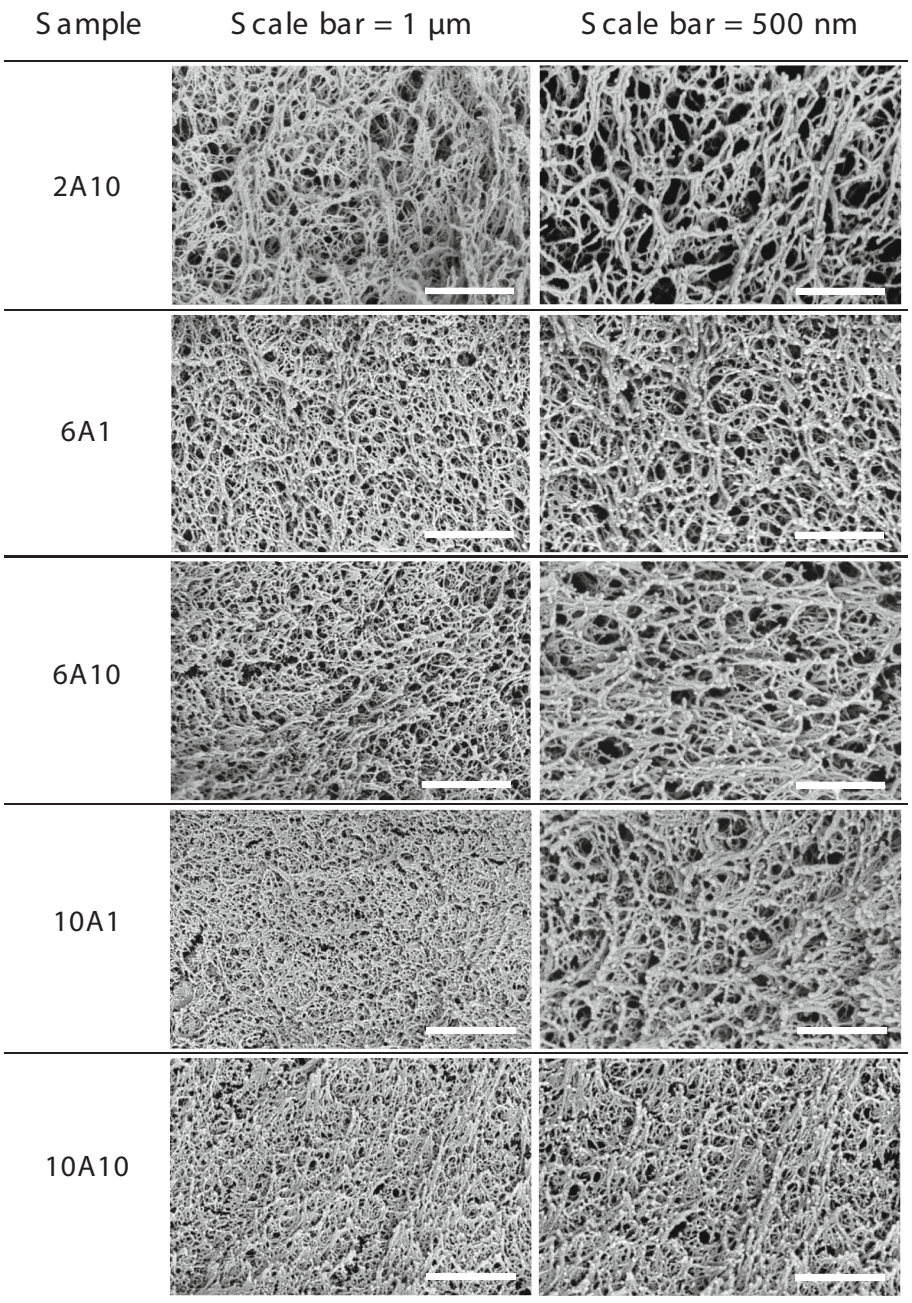

Fig. 5. SEM images of the cross-sections of agar aerogels at 50,000× mag. and scale of 1 μm (left column) and 80,000× mag. and scale of 500 nm (right column).

Table 3
Total mass loss (%) of agar aerogels during TGA analysis.

Sample[a]	Mass loss (%)[b]
2A1	69 ± 2
2A10	69 ± 2
6A1	70 ± 1
6A10	71 ± 1
10A1	73.1 ± 0.5
10A10	73.4 ± 0.2

[a] XAY, where X = agar concentration (% w/v), A = agar aerogel, and Y = ageing time (1 = 24 h; 10 = 10 days).
[b] Average of 3 measurements (mean ± SD).

degradation of the polysaccharide backbone and the decomposition of the organic matrix. Notably, TGA revealed no significant influence of agar concentration or ageing on the degradation temperature or behaviour of agar aerogels. However, a slight increase in total mass loss (~4%) was observed in samples with higher agar content, due to the greater absolute amount of degradable organic matter in these samples (Table 3).

The TGA results were further supported by the DSC analysis (Fig. 6b), which revealed two distinct thermal events. The first event, occurring between 87 °C and 144 °C, corresponded to the evaporation of residual solvents and absorbed moisture. This was characterised by a broad endothermic peak that was most pronounced in sample 10A1. This shift occurred because a denser polymer network retained more water, delaying its release. The second thermal event was characterised by a sharp exothermic peak at ≈260 °C, corresponding to the thermal degradation of the organic matter. This degradation involves the breakdown of the polysaccharide backbone, releasing higher energy.

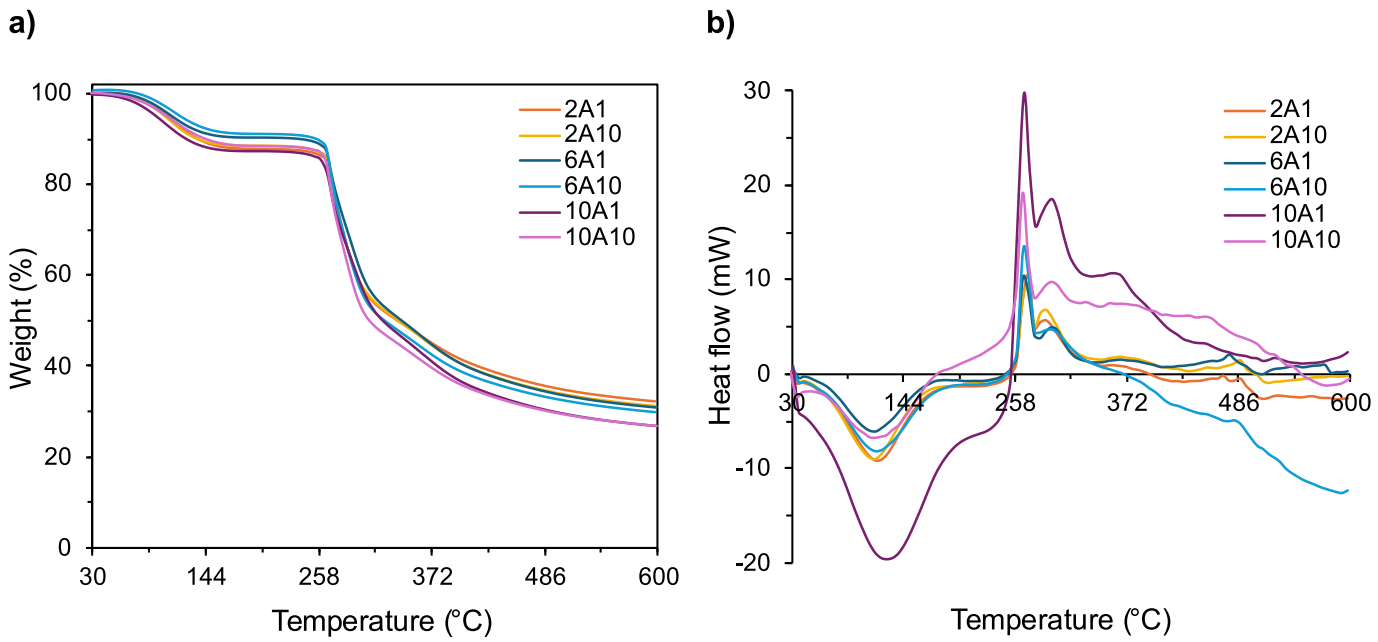

Fig. 6. a) TGA and b) DSC curves of agar aerogels.

While TGA analysis indicated similar degradation behaviour across all samples, the DSC curves revealed a clear concentration-dependent trend. Specifically, samples with higher agar content showed more intense endothermic and exothermic peaks, reflecting the greater proportion of organic matter. Contrarily, samples with lower polymer content (2A1 and 2A10) exhibited less pronounced thermal transitions. Overall, the combined thermal analyses confirmed that all agar aerogels display excellent thermal stability, with consistent and predictable degradation behaviour across varying concentrations and ageing times.

3.1.5. *Wettability*

Surface wettability, which reflects a material's hydrophobic or hydrophilic nature (Huhtamäki et al., 2018), was evaluated using the sessile drop test and a contact angle measurement.

As expected, the agar aerogels were hydrophilic (Fig. 7a). Upon deposition of water droplets on their surfaces, they spread and were rapidly absorbed by the material. Contact angle measurements confirmed this behaviour, with values ranging from 10° to 50°, indicating high surface energy and favourable wettability (Yuan & Lee, 2013).

However, the rate of water absorption was strongly influenced by agar concentration and ageing time. The 2% w/v agar aerogel (sample 2A1) exhibited superhydrophilic behaviour, completely absorbing a water droplet within 2 s. Increasing the agar concentration to 6% (sample 6A1) and 10% w/v (sample 10A1) extended the absorption time to 6 and 50 s, respectively. A similar trend was observed with prolonged ageing time: sample 6A10 absorbed the water droplet in ≈14 s, while sample 10A10 required over 1 min. Additionally, a slight oscillation of the water droplet was observed in samples 10A1 and 10A10, which may be due to a minor surface tilt or local heterogeneity.

These results demonstrate that structural changes in the aerogel matrix significantly affect surface wettability. Specifically, higher polymer concentrations and a longer ageing time led to densification of the polymer network and reduced pore diameters. Consequently, the absorption of a water droplet was delayed.

3.2. *Behaviour in aqueous media*

The behaviour of agar aerogels in aqueous media was assessed to evaluate their potential for biomedical, food or environmental applications. Their swelling capacity and stability were examined. For this purpose, two different media were selected: neutral distilled water (pH 6.9) and highly ionic SBF (pH 7.4). The samples were incubated at 25 °C, and their performance in both media was monitored over 4 weeks.

The liquid absorption capacity of the aerogels, expressed as the swelling ratio (%), was very high in both tested media (Fig. 7b, c). Around 80% of the total swelling occurred within the first 2 h of immersion, followed by a gradual increase that plateaued after 1 week. Beyond this point, no significant changes in swelling behaviour were observed. Throughout the entire measurement period, the structural integrity of the aerogels was maintained, with a moderate increase in volume and slight softening or loosening at the edges observed. There were no visible signs of degradation, indicating good dimensional stability under both neutral and highly ionic conditions.

However, the swelling behaviour was strongly influenced by the media composition. In distilled water, the maximum swelling ratio ranged from 600% (sample 10A10) to 900% (sample 6A1), whereas in SBF it was substantially lower, ranging from 250% (sample 10A10) to 450% (sample 2A10). This reduction is attributed to the higher ionic strength of SBF, which mimics the ion composition of human plasma (Kokubo & Takadama, 2006). Cations such as Na^+ and Ca^{2+} likely interacted with anionic sulphate groups in the agaropectin content of agar, forming ionic crosslinks through non-covalent interactions. These interactions restricted the mobility of the polymer chains, consequently limiting the aerogels' ability to absorb liquids (Kokubo & Takadama, 2006). This effect was particularly evident in denser aerogels, where smaller pores and reduced network flexibility further reduced liquid uptake. In contrast, distilled water, which contains few ions, enabled better polymer relaxation and greater swelling.

The agar concentration also strongly influenced the swelling behaviour. An increased agar concentration was expected to lead to decreased swelling capacity in both media, due to the formation of denser polymer networks with smaller or even inaccessible pores. This trend was observed in SBF. However, in distilled water, the 6% w/v agar aerogels showed a higher swelling ratio than the 2% w/v agar aerogels. This anomaly likely occurred due to the severe shrinkage of the 2% w/v agar aerogels, leading to partial structural collapse and a consequent reduction in swelling capacity. In contrast, 6A1 aerogels achieved a favourable balance between pore size and network integrity, enabling

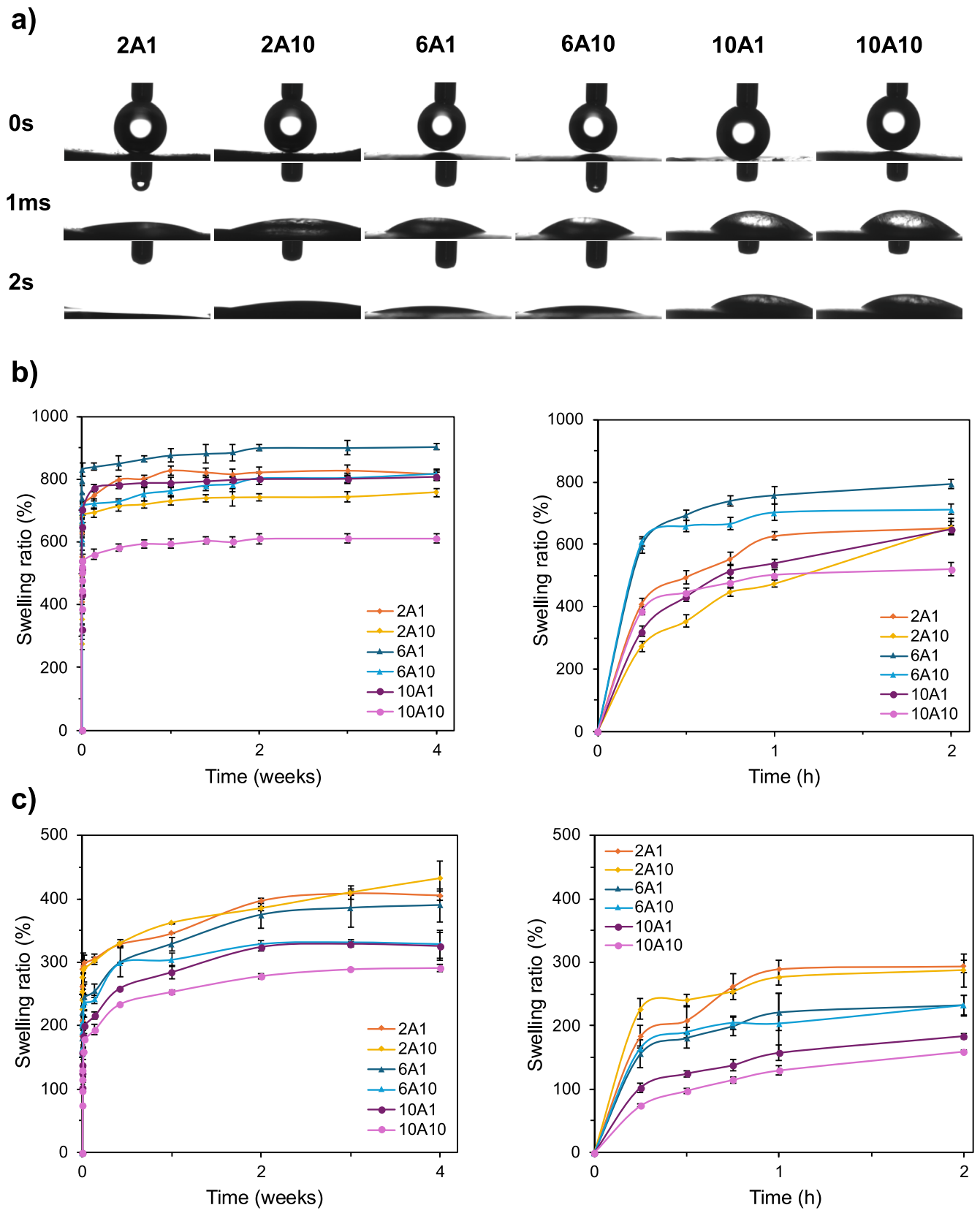

Fig. 7. a) Sessile drop test on the agar aerogels at different time points, b) swelling ratio of agar aerogels in distilled water after 4 weeks (left) and in the first 2 h (right) and c) swelling ratio of agar aerogels in SBF after 4 weeks (left) and in the first 2 h (right).

efficient, capillary-driven absorption and sustained swelling over time.

Finally, ageing time was found to have a notable impact on swelling capacity. Aerogels aged for 10 days consistently showed lower swelling ratios than those aged for only 1 day. SEM analysis revealed that prolonged ageing induced partial densification and structural changes, reducing pore accessibility and, consequently, limiting liquid uptake.

Despite differences in swelling behaviour, all the agar aerogels demonstrated excellent long-term stability in both distilled water and SBF over the 4-week testing period. They maintained their structural integrity without any visible signs of degradation.

3.3. Compressive mechanical properties

Uniaxial compression tests were performed to evaluate the elastic–-plastic behaviour of the agar aerogel samples. No brittle behaviour, such as fracture, was observed across the entire range of applied forces – from 100 N for 2% w/v agar aerogels to 450 N for 10% w/v agar aerogels (for individual compression test curves see Supplementary material, Fig. S3). Typically, biopolymer aerogels exhibit a three-phase deformation pattern in their stress-strain curves (1. linear elastic region, 2. plateau/regime of pore collapse, 3. densification) (Karadagli et al., 2015). In this work, however, this full deformation pattern was clearly identified only in 2% w/v agar aerogels (see Supplementary material, Fig. S3), as the full mechanical behaviour was not investigated for other concentrations.

Both compressive strength and compressive modulus increased significantly with higher agar concentrations (Fig. 8a, b), which can be attributed to the formation of a denser, more homogeneous fibrillar network, as supported by pore-size distribution data and SEM images. In this work, the compressive modulus was determined by linear regression over the 3%–8% strain range (see Supplementary material, Fig. S4 for individual measurements). As shown in Fig. 8b, the compressive modulus ranged from 0.2 MPa for sample 2A10 to 17.4 MPa for sample 10A1. A detailed summary of compressive modulus values for all samples is provided in the Supplementary material (Table S4). These values fall within the range typically reported for biopolymer aerogels: pectin (0.51–18 MPa) (Rege et al., 2018; Rudaz et al., 2014), cellulose (0.1–22.7 MPa) (Karadagli et al., 2015; Rege et al., 2018), κ-carrageenan (4.9–17.6 MPa) (Rege et al., 2018), and alginate (0.8–2.8 MPa) (Dosta et al., 2019). However, data on the mechanical properties of pure agar aerogels remains scarce. In contrast, agar hydrogels have been reported to exhibit much lower compressive modulus (e.g., 189 kPa) (Rahman et al., 2020), indicating the substantial enhancement in stiffness achieved in agar aerogels developed in this study.

The compressive modulus of bioaerogels is known to scale with polymer density following a power law: $E \propto \rho^n$.The exponent n is material-dependent and varies across polymer systems; for instance, reported values include $n \approx 2.8$–3.4 for cellulose and $n \approx 3$ for pectin-based aerogels (Rudaz et al., 2014; Sescousse et al., 2011). In the present study, an exponent of 2.51 was obtained (see the power-law equation and regression analysis in the Supplementary material, Fig. S5), suggesting a slightly lower dependence of stiffness on density than in other biopolymer systems.

In contrast to the effect of increasing concentration, both compressive strength and modulus decreased with prolonged ageing (Fig. 8a, b). Surprisingly, the resistance of the agar aerogels to mechanical stress is reduced, despite the observed densification of the biopolymer network. Nevertheless, the ageing process remains a relatively underexplored variable in aerogel processing, and the present findings highlight its critical role in tuning the mechanical integrity of biopolymer-based aerogels.

The energy absorbed under compression was determined from the compressive strain-stress curves at 10% and 30% strain (where applicable) and is reported in Table S6 (Supplementary material). As shown in Fig. 8c, agar aerogels effectively absorbed energy under compression, with values ranging from 0.13 kJ (sample 2A1) to 10.39 kJ (sample 10A1). The energy absorbed increased with agar concentration and decreased with prolonged ageing. These trends mirror the compressive modulus results (Fig. 8b), indicating that prolonged ageing (10 days) weakens the gel network and reduces its resistance to deformation. The difference in energy absorbed at 10% and 30% strain further highlights the strain-dependent mechanical response, while the stiffest 10% agar samples could not reach 30% strain due to their high rigidity.

To our knowledge, this study includes the first characterisation of the compressive mechanical properties of agar aerogels. A comprehensive evaluation of their overall mechanical performance, including tensile strength and elongation at break, is still required and should be investigated in future studies.

4. Conclusion

This study systematically investigated, for the first time, the influence of agar concentration and ethanol ageing time on the textural, structural, and compressive mechanical properties of agar aerogels. For highly concentrated formulations (10% w/v), a single 24-h solvent exchange step was sufficient to produce mechanically robust aerogels (Young's modulus ≈17 MPa), suitable for load-bearing or packaging applications. Notably, short ageing (1 day) increased the swelling capacity in both distilled water and SBF, regardless of agar concentration, suggesting potential for absorbent and biomedical applications. In contrast, prolonged ageing (10 days) reduced shrinkage and bulk density, while porosity and specific surface area increased by up to 25%. Among the prepared samples, the aerogels with moderate concentration (6% w/v) aged for 10 days (sample 6A10) showed the most balanced performance, combining the highest specific surface area (375 m^2/g) with excellent swelling capacity. They also exhibited favourable mechanical strength (Young's modulus ≈5 MPa) and high porosity (>90%). Although prolonged ageing improved several properties of the agar aerogels, it may not be practical for large-scale production. Our results

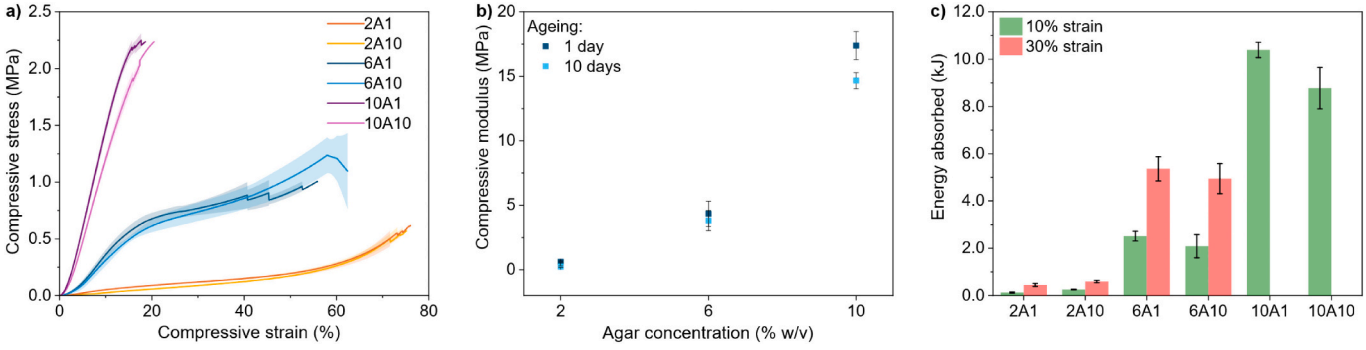

Fig. 8. Mechanical properties of agar aerogels under uniaxial compression: a) average compressive strain-stress curves, b) compressive modulus, and c) Energy absorbed under compression at 10% and 30% strain for agar aerogels (mean ± SD, $n = 4$).

indicate that the most significant improvements in agar aerogel properties occur after more than 1 day of ageing, suggesting that an intermediate ageing period (e.g., 3–5 days) could provide an optimal balance between performance and processing efficiency. Future studies should therefore examine the effects of multi-step solvent exchange at varying alcohol-to-water ratios to further refine the structure-property relationships of agar aerogels and expand their application potential. Overall, this study provides new insights into the properties of agar aerogels and demonstrates their potential as a versatile and sustainable material for various applications.

CRediT authorship contribution statement

Nika Atelšek Hozjan: Writing – review & editing, Writing – original draft, Visualization, Validation, Project administration, Methodology, Investigation, Formal analysis, Conceptualization. **Gabrijela Horvat:** Writing – review & editing, Supervision, Project administration, Methodology, Conceptualization. **Lara Gibowsky:** Writing – review & editing, Writing – original draft, Methodology, Investigation, Formal analysis. **Pavel Gurikov:** Writing – review & editing, Resources. **Željko Knez:** Writing – review & editing, Resources, Funding acquisition. **Zoran Novak:** Writing – review & editing, Supervision, Project administration, Funding acquisition.

Declaration of competing interest

The authors declare that they have no known competing financial interests or personal relationships that could have influenced the work reported in this paper.

Acknowledgements

The authors thank the Slovenian Research and Innovations Agency (ARIS) for their financial support of the Research Programme P2-0046. The authors also thank Dr. Amadeja Koler for conducting the density measurements and the Slovenian NMR centre at the National Institute of Chemistry for access to their research equipment.

Appendix A. Supplementary data

Supplementary data to this article can be found online at https://doi.org/10.1016/j.carbpol.2026.125198.

Data availability

Data will be made available on request.

References

Advancement of Materials to Sustainable and Green World. (n.d.). IAAM. Retrieved November 20, 2024, from https://www.iaamonline.org/advancement-of-materials-to-sustainable-and-green-world.

Alwin, S., & Sahaya Shajan, X. (2020). Aerogels: Promising nanostructured materials for energy conversion and storage applications. *Materials for Renewable and Sustainable Energy, 9*(2), 7. https://doi.org/10.1007/s40243-020-00168-4

Athamneh, T., Hajnal, A., Al-Najjar, M. A. A., Alshweiat, A., Obaidat, R., Awad, A. A., … Gurikov, P. (2023). In vivo tests of a novel wound dressing based on agar aerogel. *International Journal of Biological Macromolecules, 239*, Article 124238. https://doi.org/10.1016/j.ijbiomac.2023.124238

Ayyad, O., Muñoz-Rojas, D., Agulló, N., Borrós, S., & Gómez-Romero, P. (2010). High-concentration compact agar gels from hydrothermal synthesis. *Soft Matter, 6*(11), 2389–2391. https://doi.org/10.1039/B926713A

Basak, S., & Singhal, R. S. (2023). The potential of supercritical drying as a "green" method for the production of food-grade bioaerogels: A comprehensive critical review. *Food Hydrocolloids, 141*, Article 108738. https://doi.org/10.1016/j.foodhyd.2023.108738

Bertasa, M., Botteon, A., Brambilla, L., Riedo, C., Chiantore, O., Poli, T., Sansonetti, A., & Scalarone, D. (2017). Cleaning materials: A compositional multi-analytical characterization of commercial agar powders. *Journal of Analytical and Applied Pyrolysis, 125*, 310–317. https://doi.org/10.1016/j.jaap.2017.03.011

Bio-based products—European Commission. (n.d.). Retrieved November 7, 2024, from https://single-market-economy.ec.europa.eu/sectors/biotechnology/bio-based-products_en.

Buchtová, N., & Budtova, T. (2016). Cellulose aero-, cryo- and xerogels: Towards understanding of morphology control. *Cellulose, 23*(4), 2585–2595. https://doi.org/10.1007/s10570-016-0960-8

Chartier, C., Buwalda, S., Van Den Berghe, H., Nottelet, B., & Budtova, T. (2022). Tuning the properties of porous chitosan: Aerogels and cryogels. *International Journal of Biological Macromolecules, 202*, 215–223. https://doi.org/10.1016/j.ijbiomac.2022.01.042

Correa, J. P., Montalvo-Navarrete, J. M., & Hidalgo-Salazar, M. A. (2019). Carbon footprint considerations for biocomposite materials for sustainable products: A review. *Journal of Cleaner Production, 208*, 785–794. https://doi.org/10.1016/j.jclepro.2018.10.099

Cychosz, K. A., & Thommes, M. (2018). Progress in the Physisorption characterization of Nanoporous gas storage materials. *Engineering, 4*(4), 559–566. https://doi.org/10.1016/j.eng.2018.06.001

Dosta, M., Jarolin, K., & Gurikov, P. (2019). Modelling of mechanical behavior of biopolymer alginate aerogels using the bonded-particle model. *Molecules, 24*(14), Article 14. https://doi.org/10.3390/molecules24142543

García-González, C. A., Budtova, T., Durães, L., Erkey, C., Del Gaudio, P., Gurikov, P., … Smirnova, I. (2019). An opinion paper on aerogels for biomedical and environmental applications. *Molecules, 24*(9), Article 9. https://doi.org/10.3390/molecules24091815

Gavillon, R., & Budtova, T. (2008). Aerocellulose: New highly porous cellulose prepared from cellulose−NaOH aqueous solutions. *Biomacromolecules, 9*(1), 269–277. https://doi.org/10.1021/bm700972k

Gomollón-Bel, F. (2022). *IUPAC Top Ten Emerging Technologies in Chemistry 2022*.

Groult, S., & Budtova, T. (2018a). Thermal conductivity/structure correlations in thermal super-insulating pectin aerogels. *Carbohydrate Polymers, 196*, 73–81. https://doi.org/10.1016/j.carbpol.2018.05.026

Groult, S., & Budtova, T. (2018b). Tuning structure and properties of pectin aerogels. *European Polymer Journal, 108*, 250–261. https://doi.org/10.1016/j.eurpolymj.2018.08.048

Guo, J., Fu, S., Deng, Y., Xu, X., Laima, S., Liu, D., Zhang, P., Zhou, J., Zhao, H., Yu, H., Dang, S., Zhang, J., Zhao, Y., Li, H., & Duan, X. (2022). Hypocrystalline ceramic aerogels for thermal insulation at extreme conditions. *Nature, 606*(7916), 909–916. https://doi.org/10.1038/s41586-022-04784-0

Gurikov, P., Raman, S. P., Weinrich, D., Fricke, M., & Smirnova, I. (2015). A novel approach to alginate aerogels: Carbon dioxide induced gelation. *RSC Advances, 5*(11), 7812–7818. https://doi.org/10.1039/C4RA14653K

Hajnal, A., Aiyelari, M. L., Dirauf, M., & Gurikov, P. (2023). Investigation of the uniformity of gel shrinkage by imaging tracer particles using X-ray microtomography. *Advanced Engineering Materials*. , Article 2301423. https://doi.org/10.1002/adem.202301423

Horvat, G., Fajfar, T., Perva Uzunalić, A., Knez, Ž., & Novak, Z. (2017). Thermal properties of polysaccharide aerogels. *Journal of Thermal Analysis and Calorimetry, 127*(1), 363–370. https://doi.org/10.1007/s10973-016-5814-y

Horvat, G., Knez, Ž., & Novak, Z. (2015). Formation of polysaccharide aerogels in ethanol. *RSC Advances.*. https://doi.org/10.1039/C5RA14140K

Horvat, G., Pantić, M., Knez, Ž., & Novak, Z. (2022). A brief evaluation of pore structure determination for bioaerogels. *Gels, 8*(7), 438. https://doi.org/10.3390/gels8070438

Hozjan, N. A., Horvat, G., Finšgar, M., Iglesias-Mejuto, A., Palacios, I. A., García-González, C. A., … Novak, Z. (2025). Oxygen-generating and antibacterial xanthan gum/PLA aerogels loaded with dexamethasone for potential wound healing. *International Journal of Biological Macromolecules, 310*, Article 143314. https://doi.org/10.1016/j.ijbiomac.2025.143314

Huhtamäki, T., Tian, X., Korhonen, J. T., & Ras, R. H. A. (2018). Surface-wetting characterization using contact-angle measurements. *Nature Protocols, 13*(7), 1521–1538. https://doi.org/10.1038/s41596-018-0003-z

Iglesias-Mejuto, A., Magariños, B., Ferreira-Gonçalves, T., Starbird-Pérez, R., Álvarez-Lorenzo, C., Reis, C. P., … García-González, C. A. (2024). Vancomycin-loaded methylcellulose aerogel scaffolds for advanced bone tissue engineering. *Carbohydrate Polymers, 324*, Article 121536. https://doi.org/10.1016/j.carbpol.2023.121536

Jeon, Y.-J., Athukorala, Y., & Lee, J.-H. (2005). Characterization of agarose product from agar using DMSO. *Algae, 20*(1), 61–67. https://doi.org/10.4490/ALGAE.2005.20.1.061

Karadagli, I., Schulz, B., Schestakow, M., Milow, B., Gries, T., & Ratke, L. (2015). Production of porous cellulose aerogel fibers by an extrusion process. *The Journal of Supercritical Fluids, 106*, 105–114. https://doi.org/10.1016/j.supflu.2015.06.011

Karamikamkar, S., Yalcintas, E. P., Haghniaz, R., de Barros, N. R., Mecwan, M., Nasiri, R., … Khademhosseini, A. (2023). Aerogel-based biomaterials for biomedical applications: From fabrication methods to disease-targeting applications. *Advanced Science, 10*(23), Article 2204681. https://doi.org/10.1002/advs.202204681

Keil, C., Hajnal, A., Keitel, J., Kieserling, H., Rohn, S., Athamneh, T., Haase, H., & Gurikov, P. (2024). Agar aerogel powder particles for future life science applications: Fabrication and investigations on swelling behavior and cell compatibility. *Polymer Bulletin, 81*(11), 9977–9993. https://doi.org/10.1007/s00289-024-05188-y

Khoobbakht, F., Khorshidi, S., Bahmanyar, F., Hosseini, S. M., Aminikhah, N., Farhoodi, M., & Mirmoghtadaie, L. (2024). Modification of mechanical, rheological and structural properties of agar hydrogel using xanthan and locust bean gum. *Food Hydrocolloids, 147*, Article 109411. https://doi.org/10.1016/j.foodhyd.2023.109411

Kokubo, T., Kushitani, H., Sakka, S., Kitsugi, T., & Yamamuro, T. (1990). Solutions able to reproduce in vivo surface-structure changes in bioactive glass-ceramic A-W3.

Journal of Biomedical Materials Research, 24(6), 721–734. https://doi.org/10.1002/jbm.820240607

Kokubo, T., & Takadama, H. (2006). How useful is SBF in predicting in vivo bone bioactivity? *Biomaterials, 27*(15), 2907–2915. https://doi.org/10.1016/j.biomaterials.2006.01.017

Lázár, I., Čelko, L., & Menelaou, M. (2023). Aerogel-based materials in bone and cartilage tissue engineering—A review with future implications. *Gels, 9*(9), 746. https://doi.org/10.3390/gels9090746

Liao, Y., Zhang, S., Yu, S., Lu, K., Wang, M., Xiao, Y., & Ding, F. (2024). Microstructural evolution of bio-based chitosan aerogels for thermal insulator with superior moisture/fatigue resistance and anti-thermal-shock. *International Journal of Biological Macromolecules, 278*, Article 134681. https://doi.org/10.1016/j.ijbiomac.2024.134681

Mao, J., Iocozzia, J., Huang, J., Meng, K., Lai, Y., & Lin, Z. (2018). Graphene aerogels for efficient energy storage and conversion. *Energy & Environmental Science, 11*(4), 772–799. https://doi.org/10.1039/C7EE03031B

Méndez, D. A., Schroeter, B., Martínez-Abad, A., Fabra, M. J., Gurikov, P., & López-Rubio, A. (2023). Pectin-based aerogel particles for drug delivery: Effect of pectin composition on aerogel structure and release properties. *Carbohydrate Polymers, 306*, Article 120604. https://doi.org/10.1016/j.carbpol.2023.120604

Mostafavi, F. S., & Zaeim, D. (2020). Agar-based edible films for food packaging applications—A review. *International Journal of Biological Macromolecules, 159*, 1165–1176. https://doi.org/10.1016/j.ijbiomac.2020.05.123

Novak, Z., & Knez, Ž. (1997). Diffusion of methanol–liquid CO2 and methanol–supercritical CO2 in silica aerogels. *Journal of Non-Crystalline Solids, 221*(2), 163–169. https://doi.org/10.1016/S0022-3093(97)00342-6

Pantić, M., Nowak, M., Lavrič, G., Knez, Ž., Novak, Z., & Zizovic, I. (2024). Enhancing the properties and morphology of starch aerogels with nanocellulose. *Food Hydrocolloids, 156*, Article 110345. https://doi.org/10.1016/j.foodhyd.2024.110345

Paul, J., & Ahankari, S. S. (2023). Nanocellulose-based aerogels for water purification: A review. *Carbohydrate Polymers, 309*, Article 120677. https://doi.org/10.1016/j.carbpol.2023.120677

Paul, J., Qamar, A., Ahankari, S. S., Thomas, S., & Dufresne, A. (2024). Chitosan-based aerogels: A new paradigm of advanced green materials for remediation of contaminated water. *Carbohydrate Polymers, 338*, Article 122198. https://doi.org/10.1016/j.carbpol.2024.122198

Payanda Konuk, O., Alsuhile, A. A. A. M., Yousefzadeh, H., Ulker, Z., Bozbag, S. E., García-González, C. A., … Erkey, C. (2023). The effect of synthesis conditions and process parameters on aerogel properties. *Frontiers in Chemistry, 11*, Article 1294520. https://doi.org/10.3389/fchem.2023.1294520

Rahman, J. M. H., Shiblee, M. N. I., Ahmed, K., Khosla, A., Kawakami, M., & Furukawa, H. (2020). Rheological and mechanical properties of edible gel materials for 3D food printing technology. *Heliyon, 6*(12), Article e05859. https://doi.org/10.1016/j.heliyon.2020.e05859

Ratke, L., & Gurikov, P. (2021). *The chemistry and physics of aerogels*. Cambridge University Press. https://doi.org/10.1017/9781108778336

Rege, A., Preibisch, I., Schestakow, M., Ganesan, K., Gurikov, P., Milow, B., … Itskov, M. (2018). Correlating synthesis parameters to morphological entities: Predictive modeling of biopolymer aerogels. *Materials, 11*(9), Article 9. https://doi.org/10.3390/ma11091670

Robitzer, M., David, L., Rochas, C., Di Renzo, F., & Quignard, F. (2008). Nanostructure of calcium alginate aerogels obtained from multistep solvent exchange route. *Langmuir, 24*(21), 12547–12552. https://doi.org/10.1021/la802103t

Robitzer, M., Renzo, F. D., & Quignard, F. (2011). Natural materials with high surface area. Physisorption methods for the characterization of the texture and surface of polysaccharide aerogels. *Microporous and Mesoporous Materials, High Surface Area Porous Materials, 140*(1), 9–16. https://doi.org/10.1016/j.micromeso.2010.10.006

Robitzer, M., Tourrette, A., Horga, R., Valentin, R., Boissière, M., Devoisselle, J. M., … Quignard, F. (2011). Nitrogen sorption as a tool for the characterisation of polysaccharide aerogels. *Carbohydrate Polymers, 85*(1), 44–53. https://doi.org/10.1016/j.carbpol.2011.01.040

Rudaz, C., Courson, R., Bonnet, L., Calas-Etienne, S., Sallée, H., & Budtova, T. (2014). Aeropectin: Fully biomass-based mechanically strong and thermal superinsulating aerogel. *Biomacromolecules, 15*(6), 2188–2195. https://doi.org/10.1021/bm500345u

Selvasekaran, P., & Chidambaram, R. (2022). Bioaerogels as food materials: A state-of-the-art on production and application in micronutrient fortification and active packaging of foods. *Food Hydrocolloids, 131*, Article 107760. https://doi.org/10.1016/j.foodhyd.2022.107760

Sescousse, R., Gavillon, R., & Budtova, T. (2011). Aerocellulose from cellulose–ionic liquid solutions: Preparation, properties and comparison with cellulose–NaOH and cellulose–NMMO routes. *Carbohydrate Polymers, 83*(4), 1766–1774. https://doi.org/10.1016/j.carbpol.2010.10.043

Sing, K. S. W. (1982). Reporting physisorption data for gas/solid systems with special reference to the determination of surface area and porosity (provisional). *Pure and Applied Chemistry, 54*(11), 2201–2218. https://doi.org/10.1351/pac198254112201

Smirnova, I., & Gurikov, P. (2018). Aerogel production: Current status, research directions, and future opportunities. *The Journal of Supercritical Fluids, 30th Year Anniversary Issue of the Journal of Supercritical Fluids, 134*, 228–233. https://doi.org/10.1016/j.supflu.2017.12.037

Subrahmanyam, R., Gurikov, P., Dieringer, P., Sun, M., & Smirnova, I. (2015). On the road to biopolymer aerogels—Dealing with the solvent. *Gels, 1*(2), Article 2. https://doi.org/10.3390/gels1020291

Subrahmanyam, R., Keil, C., Dieringer, P., Hübner, C., Bueno Morales, A., Gurikov, P., Nissen, J., Holtkamp, M., Karst, U., Haase, H., & Smirnova, I. (2019). Alginate aerogels carrying calcium, zinc and silver cations for wound care: Fabrication and metal detection. *The Journal of Supercritical Fluids, 153*, Article 104545. https://doi.org/10.1016/j.supflu.2019.104545

Thommes, M., Kaneko, K., Neimark, A. V., Olivier, J. P., Rodriguez-Reinoso, F., Rouquerol, J., & Sing, K. S. W. (2015). Physisorption of gases, with special reference to the evaluation of surface area and pore size distribution (IUPAC technical report). *Pure and Applied Chemistry, 87*(9–10), 1051–1069. https://doi.org/10.1515/pac-2014-1117

Usov, A. I. (1998). Structural analysis of red seaweed galactans of agar and carrageenan groups. *Food Hydrocolloids, 12*(3), 301–308. https://doi.org/10.1016/S0268-005X(98)00018-6

Veronovski, A., Tkalec, G., Knez, Ž., & Novak, Z. (2014). Characterisation of biodegradable pectin aerogels and their potential use as drug carriers. *Carbohydrate Polymers, 113*, 272–278. https://doi.org/10.1016/j.carbpol.2014.06.054

Yuan, Y., & Lee, T. R. (2013). Contact angle and wetting properties. In G. Bracco, & B. Holst (Eds.), *Surface Science Techniques* (pp. 3–34). Springer. https://doi.org/10.1007/978-3-642-34243-1_1.

Zou, F., & Budtova, T. (2021). Polysaccharide-based aerogels for thermal insulation and superinsulation: An overview. *Carbohydrate Polymers, 266*, Article 118130. https://doi.org/10.1016/j.carbpol.2021.118130